

Fi²VTS: TIME SERIES FORECASTING VIA CAPTURING INTRA- AND INTER-VARIABLE VARIATIONS IN THE FREQUENCY DOMAIN

A PREPRINT

 **Rujia Shen**

Faculty of Computing
Harbin Institute of Technology
Harbin, Heilongjiang, China
shenrujia@stu.hit.edu.cn

Yang Yang

School of Artificial Intelligence
Changchun University of Science and Technology
Changchun, Jilin, China
yangyang_hit_wi@163.com

Yaoxiong Lin

Faculty of Computing
Harbin Institute of Technology
Harbin, Heilongjiang, China
23S136168@stu.hit.edu.cn

Liangliang Liu

Faculty of Computing
Harbin Institute of Technology
Harbin, Heilongjiang, China
liull@stu.hit.edu.cn

Boran Wang

Faculty of Computing
Harbin Institute of Technology
Shenzhen, Guangdong, China
wangboran@hit.edu.cn

Yi Guan

Faculty of Computing
Harbin Institute of Technology
Harbin, Heilongjiang, China
guanyi@hit.edu.cn

 **Jingchi Jiang**

The Artificial Intelligence Institute
Harbin Institute of Technology
Harbin, Heilongjiang, China
jiangjingchi@hit.edu.cn

October 4, 2024

ABSTRACT

Time series forecasting (TSF) plays a crucial role in various applications, including medical monitoring and crop growth. Despite the advancements in deep learning methods for TSF, their capacity to predict long-term series remains constrained. This limitation arises from the failure to account for both intra- and inter-variable variations meanwhile. To mitigate this challenge, we introduce the Fi²VBlock, which leverages a Frequency domain perspective to capture intra- and inter-variable Variations. After transforming into the frequency domain via the Frequency Transform Module, the Frequency Cross Attention between the real and imaginary parts is designed to obtain enhanced frequency representations and capture intra-variable variations. Furthermore, Inception blocks are employed to integrate information, thus capturing correlations across different variables. Our backbone network, Fi²VTS, employs a residual architecture by concatenating multiple Fi²VBlocks, thereby preventing degradation issues. Theoretically, we demonstrate that Fi²VTS achieves a substantial reduction in both time and memory complexity, decreasing from $\mathcal{O}(L^2)$ to $\mathcal{O}(L)$ per Fi²VBlock computation. Empirical evaluations reveal that Fi²VTS outperforms other baselines on two benchmark datasets. The implementation code is accessible at <https://github.com/HITshenrj/Fi2VTS>.

Keywords Time series forecasting · Frequency Transform Module · Frequency Cross Attention · Residual structure · Frequency domain

1 Introduction

Time series forecasting (TSF) aims to forecast the future value of time series using their historical values. With the development of deep learning, numerous models have been proposed and achieved superior performance [Wu et al., 2021, Liu et al., 2022, Zhou et al., 2022, Woo et al., 2022, Nie et al., 2023, Liu et al., 2024, Xu et al., 2024]. The application of these models in the real world spans various sectors, such as medical treatment [Li et al., 2021, Khadem et al., 2023] and agriculture [Saini et al., 2020]. These existing models generally either focus on the intra-variable variations by using channel independence [Nie et al., 2023], or simply apply attention in the time or frequency domain to capture inter-variable variations [Wu et al., 2021, Liu et al., 2022, Zhou et al., 2022, Woo et al., 2022, Liu et al., 2024, Xu et al., 2024].

However, mutual influences between variables are of equal importance to intra-variable variations. As illustrated in Figure 1, intra-variable variations refer to the changes within each variable over time, while inter-variable variations denote the mutual influences between different variables. For instance, when predicting blood glucose, not only does historical blood glucose play a role, but historical records of diet are also critical for determining future blood glucose changes. Previous research [Zhang and Yan, 2023] has attempted to address this issue by exploring and leveraging both intra- and inter-variable dependencies in the time domain. Nonetheless, a potentially more fundamental approach is to directly and simultaneously capture these variations in the frequency domain, enabling the modeling of the intrinsic properties of the time series. This frequency-domain approach can provide a more robust framework for understanding the underlying dynamics of the data, potentially leading to more accurate forecasting.

To capture intra- and inter-variable variations directly and simultaneously, we propose Fi^2VTS , which shifts our perspective to the Frequency domain to capturing intra- and inter-variable Variations for Time Series forecasting. First, based on the fact that real-world time series often exhibit multi-periodicity, such as daily and annual variations in electricity transformations, unlike other TSF methods [Zhou et al., 2022, Yi et al., 2023] using the Fast Fourier Transform (FFT), we propose to use the Short-Time Fourier Transform (STFT) with predefined windows of varying sizes in the Frequency Transform Module. This approach aims to decouple overlapping and interacting periodic signals, thereby better addressing both intra- and inter-variable variations. Second, inspired by the inherent Kramer-Kronig relations (KKRs) in the frequency domain, we introduce a novel Frequency Cross Attention. This mechanism operates between the real and imaginary parts of the frequency representation, thereby enhancing the frequency representations and capturing intra-variable variations more effectively. Moreover, we employ Inception blocks to extract changes between variables, which further improve the model’s ability to handle inter-variable dependencies. These above components form Fi^2VBlock , which serves as the fundamental building block of Fi^2VTS . The overall architecture of Fi^2VTS adopts a residual structure by stacking multiple Fi^2VBlock s. This design not only enhances the model’s capacity to learn complex patterns but also mitigates degradation problems, ensuring robust performance in long-term forecasting tasks.

Our contributions are four-fold:

- Motivated by the inherent KKR in the frequency domain, we develop a modular framework for modeling both intra- and inter-variable variations. Once transforming into the frequency domain, we can present these variations simultaneously.
- We propose Fi^2VTS , which is built upon residual Fi^2VBlock s. Each Fi^2VBlock first decouples multiple periodic signals using the Short-Time Fourier Transform (STFT), then captures intra-variable variations through Frequency Cross Attention between the real and imaginary parts. Lastly, the Fi^2VBlock employs Inception blocks to mix information, capturing correlations between variables effectively.
- We significantly reduce both the time complexity and memory complexity for each Fi^2VBlock computation from $\mathcal{O}(L^2)$ to $\mathcal{O}(L)$, as verified through theoretical analysis and empirical evaluations.

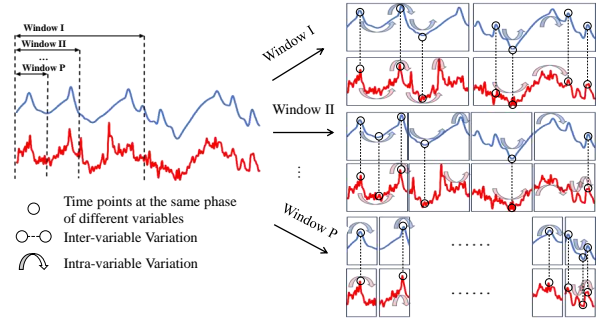


Figure 1: Intra- and inter-variable variations. Intra-variable variations refer to the changes within each variable over time, while inter-variable variations denote the interactions between different variables. Predefined windows can decouple overlapping and interacting periodic signals, thereby better addressing both intra- and inter-variable variations.

- Experimental results demonstrate that Fi²VTS consistently achieves state-of-the-art performance in time series forecasting. The model shows reduction in Mean Squared Error (MSE) and Mean Absolute Error (MAE) compared to existing methods on medical and agricultural fields.

2 Related Work and Motivation

In this section, we commence by presenting the problem statement, as detailed in Section 2.1. Subsequently, we discuss the cutting-edge TSF methods (Section 2.2), which, despite their remarkable performances, still offer the potential for further refinement. In Section 2.3, we elaborate on the method for converting time-domain information into the frequency domain. Finally, in Section 2.4, we delve into the Kramers-Kronig relations between the real and imaginary components of causal systems in the frequency domain, which serve as both the inspiration and theoretical underpinning of our research.

2.1 Problem Statement

The input data points, denoted by $X = \{x_1^t, \dots, x_D^t\}_{t=1}^L \in \mathbb{R}^{D \times L}$, are defined as the lookback window of time series, where L represents the length of the lookback window, $D \geq 1$ is the number of variables, and x_j^t is the value of the j -th variable at the t -th time step. The task of TSF is to predict the forecasting horizon $\hat{X} = \{\hat{x}_1^t, \dots, \hat{x}_D^t\}_{t=L+1}^{L+T} \in \mathbb{R}^{D \times T}$ by using the lookback window. In this paper, we specifically focus on multi-step TSF, where $T > 1$.

2.2 Time Series Forecasting

Many classical methods, such as ARIMA [Box and Jenkins, 1968, Box et al., 2015], followed a Markovian process and constructed autoregressive TSF models based on predefined time patterns. However, this autoregressive process became ineffective in real-world nonlinear and non-stationary conditions.

With the flourishing development of deep neural networks, RNNs, specialized for time series data analysis, have been proposed and achieved remarkable results. The simplest form in the RNN family [Medsker and Jain, 2001] contains a single hidden layer and recurrent connections. However, this form often suffers from the problems of vanishing or exploding gradient, which makes it challenging for long-term series prediction [Bengio et al., 1994]. To address the gradient problems, Long Short-Term Memory (LSTM) [Hochreiter and Schmidhuber, 1997] and Gated Recurrent Unit (GRU) [Chung et al., 2014] employ gated structures to control the flow of information, allowing better handling of dependencies in long sequences. However, due to inherent design flaws, recurrent models still need help adapting to long-term TSF tasks.

With the resounding success of the Transformer architecture in the fields of natural language processing [Vaswani et al., 2017, Kenton and Toutanova, 2019] and computer vision [Dosovitskiy et al., 2020], it has also been refined and adapted for TSF. Autoformer [Wu et al., 2021] introduced an auto-correlation mechanism based on series periodicity, facilitating dependency discovery and representation aggregation at the sub-series level. This innovation enhanced the Transformer’s information utilization and effectively eliminated the information utilization bottleneck. NSformer [Liu et al., 2022] sought to improve the forecasting capability for non-stationary data by introducing series stationarization and de-stationary attention mechanisms, demonstrating its efficacy through theoretical analysis and empirical experiments. To further enhance the accuracy and efficiency of Transformer-based predictions, ETSformer [Woo et al., 2022] leveraged the principle of exponential smoothing. It employed exponential smoothing and frequency attention instead of the self-attention mechanism in traditional Transformers, aiming to improve accuracy and efficiency. PatchTST [Nie et al., 2023] utilized a patching design to preserve local semantic information in the embeddings while concurrently reducing the computation and memory usage of the attention maps quadratically, enabling the model to attend to a longer historical context. To adapt the Transformer for handling longer lookback windows and to eliminate meaningless attention maps, iTransformer [Liu et al., 2024] reconfigured the Transformer architecture by simply applying the attention and feed-forward networks to the inverted dimensions. This modification allowed for more efficient processing of longer sequences and improved attention mechanisms. FEDformer [Zhou et al., 2022] emphasized enhancing the Transformer’s capability to capture the global profile of time series by performing seasonal-trend decomposition in the frequency domain. To improve the Transformer’s ability to model cross-time and cross-dimension dependencies, Crossformer [Zhang and Yan, 2023] initially segmented the time series while preserving both temporal and dimensional information. It then employed a two-stage attention mechanism to capture cross-time and cross-dimension dependencies individually, offering a more nuanced and comprehensive understanding of the time series.

Not only has the Transformer architecture been applied to time series forecasting, but CNN-based methods have also proven highly efficient. TimesNet [Wu et al., 2023] leveraged convolutional neural networks to identify multi-periodicity in time series, effectively extracting complex temporal variations through a parameter-efficient inception block [Szegedy

et al., 2015]. Recently, a series of MLP-based methods have been proposed to reduce model parameters and enhance computational speed while maintaining accuracy. LightTS [Zhang et al., 2022], based on the notion that down-sampling a time series often preserves the majority of its information, used an MLP-based structure to make predictions after down-sampling, significantly reducing computational load without compromising accuracy. DLinear [Zeng et al., 2023] avoided the temporal information loss caused by the permutation-invariant self-attention mechanism by employing a simple one-layer linear model, achieving greater accuracy than Transformer-based models. FreTS [Yi et al., 2023] applied MLPs in the frequency domain, allowing them to have a complete view of signals and more easily learn global dependencies. FITS [Xu et al., 2024] transformed the time series into the complex frequency domain for frequency interpolation and subsequently mapped the interpolation back to the time domain. FITS used a single linear layer to learn the interpolation of complex values.

Although the methods mentioned above effectively predict time series, they overlook intra- and inter-variable variations in the frequency domain, which constrains their capacity to predict long-term time series. Consequently, this paper aims to address this shortcoming by exploring how to simultaneously capture both intra- and inter-variable variations in the frequency domain.

2.3 From the Time Domain to the Frequency Domain

A commonly used method for transforming time series data from the time domain to the frequency domain is the Fast Fourier Transform (FFT) [Nussbaumer and Nussbaumer, 1982, Cochran et al., 1967]. The FFT is widely applied because it significantly reduces the computational complexity of the Discrete Fourier Transform [Briggs and Henson, 1995]. In this study, however, we use the Short Time Fourier Transform (STFT) [Cvetkovic, 2000, Durak and Arıkan, 2003] to decouple overlapping and interacting periodic signals, thereby better accounting for intra- and inter-variable variations.

The STFT consists of multiple windows of different sizes, and its fundamental component is the Fourier transform. Therefore, the STFT can be considered a collection of numerous Fourier transforms. The STFT first divides a long time series into shorter segments of equal length and then computes the Fourier transform separately for each segment. As the window slides along the time axis, until it reaches the end, the STFT of the time series is computed, resulting in a two-dimensional representation of the series. Moreover, different window sizes produce multi-scale STFT results.

Mathematically, this process can be expressed as follows:

$$\text{STFT}\{X\}(\omega, \tau) = \sum_{t=1}^L x^t w(t - \tau) e^{-i\omega t}, \quad (1)$$

where $w(\tau)$ represents the window function, usually a Hann window, X denotes the time series to transform and ω is the angular frequency with $i^2 = -1$. The $\text{STFT}\{X\}$ represents a function that captures the variations of the signal concerning both the time and frequency domain.

2.4 The Relations between Real and Imaginary Components in the Frequency Domain

In control theory, a causal system is defined as one in which the output depends on past and present inputs but not on future ones [Karimi and Hamilton, 2003]. This relationship aligns with the inherent nature of time series data, where data unfolds sequentially over time, and present data points do not precede future ones. Consequently, in this study, we approximate the inherent mechanism of time series data as a causal system for analysis.

We will subsequently elucidate a theoretical constraint on a causal system in the frequency domain, explicitly concerning the interdependence of the real and imaginary parts as described by the Kramers-Kronig relations [King, 2009]. These relations are pivotal in linking the real and imaginary components of an analytic and causal function. Essentially, they provide integral transforms that describe how the real part of a function can be derived from its imaginary part and vice versa, given the function’s causality and analyticity.

Theorem 1 *Let $X(t)$ be a causal time function with respect to time t , i.e., $X(t) = \begin{cases} 0, & t < 0 \\ X(t), & t \geq 0 \end{cases}$. $X(t)$ does*

not contain the continuous-time unit impulse function $\delta(t) = \begin{cases} 0, & t \neq 0 \\ \infty, & t = 0 \end{cases}$ and derivatives at $t = 0$. Suppose the Fourier transform \mathcal{F} of $X(t)$ is represented in the form of the real part Re and the imaginary part Im , i.e., $X(t) \leftrightarrow F(\omega) = Re(\omega) + iIm(\omega)$. Then, we have:

$$\begin{aligned} \text{Re}(\omega) &= \frac{1}{\pi} \int_{-\infty}^{\infty} \frac{\text{Im}(\sigma)}{\omega - \sigma} d\sigma, \\ \text{Im}(\omega) &= -\frac{1}{\pi} \int_{-\infty}^{\infty} \frac{\text{Re}(\sigma)}{\omega - \sigma} d\sigma. \end{aligned} \quad (2)$$

The Equation 2 [Cizek, 1970, Benitez et al., 2001] asserts that for any causal time function, the real and imaginary components of its Fourier transform adhere to the Kramers-Kronig relations (KKRs). These relations establish bidirectional mathematical connections between the real and imaginary parts of complex functions. From Equation 2, it can be observed that the real and imaginary parts exhibit periodic characteristics as a function of ω . Moreover, the real and imaginary parts themselves can reflect intra-variable characteristics of time series, thereby making their expression conducive to effective forecasting.

Next, we will demonstrate the Kramers-Kronig relationship within the context of the Short-Time Fourier Transform (STFT) to elucidate the design motivation of our method. Although both frequency and time are localized in STFT, this proof can indirectly validate the rationality and foundation of our model design.

Lemma 1 *Let $X(t)$ be a causal time function with respect to time t , i.e., $X(t) = \begin{cases} 0, & t < 0 \\ X(t), & t \geq 0 \end{cases}$. $X(t)$ does not contain the continuous-time unit impulse function $\delta(t) = \begin{cases} 0, & t \neq 0 \\ \infty, & t = 0 \end{cases}$ and derivatives at $t = 0$. Suppose the STFT of $X(t)$ is represented in the form of the real part Re and the imaginary part Im with window w , which is centered at τ , i.e., $X(t) \leftrightarrow \text{STFT}(\omega, \tau) = \text{Re}(\omega, \tau) + i\text{Im}(\omega, \tau)$. Then, we have:*

$$\begin{aligned} \text{Re}(\omega, \tau) &= \frac{1}{\pi} \int_{-\infty}^{\infty} \frac{\text{Im}(\sigma, \tau)}{\omega - \sigma} d\sigma, \\ \text{Im}(\omega, \tau) &= -\frac{1}{\pi} \int_{-\infty}^{\infty} \frac{\text{Re}(\sigma, \tau)}{\omega - \sigma} d\sigma. \end{aligned} \quad (3)$$

Proof 1 $X(t)$ can be expressed as $X(t) = X(t)\epsilon(t)$ by introducing the unit step function $\epsilon(t) = \begin{cases} 1, & t > 0 \\ 0, & t \leq 0 \end{cases}$. Taking the STFT of both sides of $X(t) = X(t)\epsilon(t)$, based on the frequency domain convolution theorem [Weisstein, 2014], we have:

$$\begin{aligned} \text{STFT}\{X(t)\} &= \text{Re}(\omega, \tau) + i\text{Im}(\omega, \tau), \\ \text{STFT}\{X(t)\epsilon(t)\} &= \frac{1}{2\pi} [\text{Re}(\omega, \tau) + i\text{Im}(\omega, \tau)] \times [\pi\delta(\omega) + \frac{1}{i\omega}]. \end{aligned} \quad (4)$$

Using $\text{STFT}\{X(t)\} = \text{STFT}\{X(t)\epsilon(t)\}$ and then we have:

$$\begin{aligned} \text{Re}(\omega, \tau) + i\text{Im}(\omega, \tau) &= \frac{1}{2\pi} [\text{Re}(\omega, \tau) + i\text{Im}(\omega, \tau)] \times [\pi\delta(\omega) + \frac{1}{i\omega}] \\ &= [\frac{\text{Re}(\omega, \tau)}{2} + \frac{1}{2\pi} \text{Im}(\omega, \tau) \times \frac{1}{\omega}] + i[\frac{\text{Im}(\omega, \tau)}{2} - \frac{1}{2\pi} \text{Re}(\omega, \tau) \times \frac{1}{\omega}]. \end{aligned} \quad (5)$$

Equating the real and imaginary parts on both sides of the equation and rearranging, we get:

$$\begin{aligned} \text{Re}(\omega, \tau) &= \frac{1}{\pi} \text{Im}(\omega, \tau) \times \frac{1}{\omega} = \frac{1}{\pi} \int_{-\infty}^{\infty} \frac{\text{Im}(\sigma, \tau)}{\omega - \sigma} d\sigma, \\ \text{Im}(\omega, \tau) &= -\frac{1}{\pi} \text{Re}(\omega, \tau) \times \frac{1}{\omega} = -\frac{1}{\pi} \int_{-\infty}^{\infty} \frac{\text{Re}(\sigma, \tau)}{\omega - \sigma} d\sigma. \end{aligned} \quad (6)$$

So far, the Equation 3 has been proven.

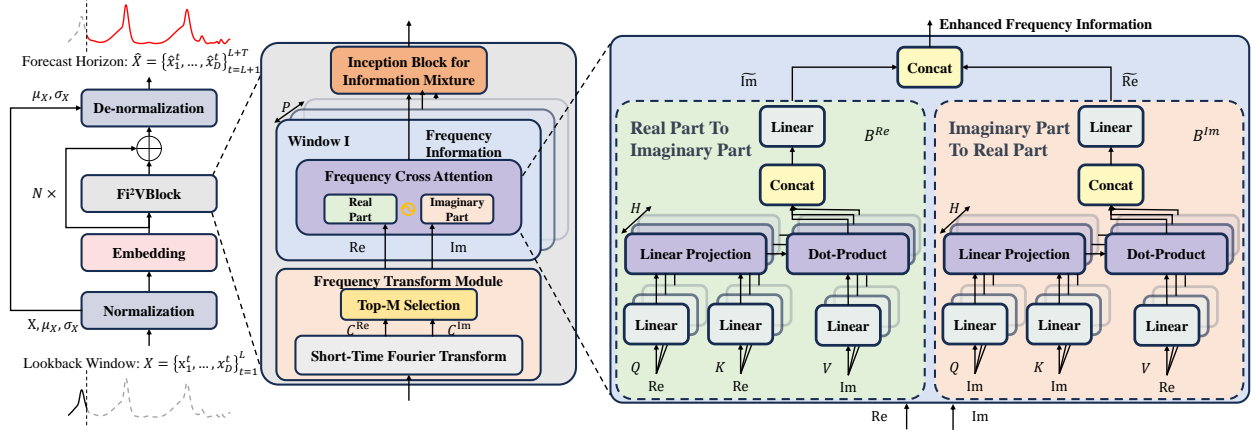


Figure 2: The structure of Fi^2VTS . Initially, the input lookback window, $X \in \mathbb{R}^{D \times L}$, undergoes normalization and embedding processes to transform it into $X^0 \in \mathbb{R}^{E \times L}$. This transformed input is then fed into a series of residual Fi^2VBlock s. The output of the N -th Fi^2VBlock , after undergoing denormalization, results in the forecasting horizon $\hat{X} \in \mathbb{R}^{D \times T}$. The n -th Fi^2VBlock is defined as $X^n = \text{Fi}^2\text{VBlock}^n(X^{n-1}) + X^{n-1}$. The process within each Fi^2VBlock begins with the application of the STFT, utilizing Equation 7 to the time series data with varying window sizes. This step decomposes the data into its corresponding real and imaginary components in the frequency domain, which is then processed through the Top-M frequency selection as described in Equation 9. Subsequently, the Fi^2VBlock captures intra-variable variations using Frequency Cross Attention between the real and imaginary parts and obtain the enhanced real part $\tilde{\text{Re}}$ and the imaginary part $\tilde{\text{Im}}$. Finally, the Fi^2VBlock integrates inter-variable information through parameter-efficient Inception blocks, completing the transformation process within the block.

Inspired by the fact that the KKR's remain valid in the context of STFT, we can derive a multi-scale representation and multi-frequency components of time series through STFT. This transformation enhances computational efficiency and significantly reduces the computational cost of time series analysis [Xu et al., 2020]. Subsequently, by adaptively modeling the transformations between the real and imaginary parts, we can further capture intra-variable variations, which characterize the properties of time series variables in the frequency domain.

3 Fi^2VTS

In this section, we introduce the Fi^2VTS , as illustrated in Figure 2, which features a modular architecture specifically designed to model intra- and inter-variable variations in the frequency domain. We apply the normalization at the very beginning of Fi^2VTS to address the nonstationary characteristics resulting from varying mean and standard deviation. At the end of the Fi^2VTS , denormalization is applied to transform the model outputs back to the original statistics. Then, the Fi^2VTS incorporates a series of residual-connected Fi^2VBlock s. These Fi^2VBlock s initially utilize the Frequency Transform Module, followed by the Frequency Cross Attention mechanism to dynamically allocate attention weights to the real and imaginary components associated with intra-variable variations. Additionally, the Fi^2VBlock s integrate inter-variable information efficiently through parameter-efficient Inception blocks.

3.1 Frequency Transform Module

The Frequency Transform Module transforms the input into frequency components using the STFT:

$$C_{j,p,k} = \text{STFT}\{X_j\}(\omega_k, \tau_p) = \sum_{t=1}^L x_j^t w_p(t - \tau_p) e^{-i\omega_k t}, \quad (7)$$

where X_j represent the time series corresponding to the j -th variable, $w_p(\tau_p)$ denotes the p -th window function centered at τ_p with a total of P window functions. These window functions are collectively represented as $\{w_p\}_{p=1, \dots, P}$. The k -th angular frequency is denoted by ω_k . $C_{j,p,k}$ signifies the k -th result of the STFT applied to the j -th time series using the p -th predefined window function, encapsulating the real and imaginary components. The STFT, referred to

as Equation 7, can be decomposed into its real and imaginary parts utilizing $e^{-i\omega_k t} = \cos(-\omega_k t) + i \sin(-\omega_k t) = \cos(\omega_k t) - i \sin(\omega_k t)$. This decomposition yields the following formulations:

$$\begin{aligned} C_{j,p,k}^{\text{Re}} &= \sum_{t=1}^L x_j^t w_p(t - \tau_p) \cos \omega_k t, \\ C_{j,p,k}^{\text{Im}} &= - \sum_{t=1}^L x_j^t w_p(t - \tau_p) \sin \omega_k t, \end{aligned} \quad (8)$$

where $C_{j,p,k}^{\text{Re}}$ and $C_{j,p,k}^{\text{Im}}$ represent the k -th real and imaginary components, respectively, of the j -th time series, which are derived through decomposition using the p -th window function. Given the sparsity characteristic of the frequency domain, we opt to select only the Top-M amplitude values to mitigate the computational load of the attention mechanism. Consequently, we identify the most significant real components $C_{j,p,1}^{\text{Re}}, \dots, C_{j,p,M}^{\text{Re}}$ and imaginary components $C_{j,p,1}^{\text{Im}}, \dots, C_{j,p,M}^{\text{Im}}$, with M being a hyperparameter. Furthermore, by concatenating the components obtained across all P windows, we form the matrices $\text{Re} \in \mathbb{R}^{D \times P \times M}$ and $\text{Im} \in \mathbb{R}^{D \times P \times M}$ with $\text{Amp}(\cdot)$ denoting the amplitude values:

$$\begin{aligned} \{C_{j,p,1}^{\text{Re}}, \dots, C_{j,p,M}^{\text{Re}}\}, \{C_{j,p,1}^{\text{Im}}, \dots, C_{j,p,M}^{\text{Im}}\} &= \arg \text{Top-M}(\text{Amp}(C_{j,p,k}^{\text{Re}}, C_{j,p,k}^{\text{Im}})), \\ &\quad k \in \{1, \dots, M\} \\ \text{Re} &= \text{Concatenate}_{j \in \{1, \dots, D\}, p \in \{1, \dots, P\}, m \in \{1, \dots, M\}} (C_{j,p,m}^{\text{Re}}), \\ \text{Im} &= \text{Concatenate}_{j \in \{1, \dots, D\}, p \in \{1, \dots, P\}, m \in \{1, \dots, M\}} (C_{j,p,m}^{\text{Im}}). \end{aligned} \quad (9)$$

3.2 Frequency Cross Attention

Based on the Lemma 1, once the STFT is performed, the imaginary part can be derived from the corresponding real part, and vice versa. The crux of our method is to compute an importance score between the real and imaginary parts of each variable. To this end, we design the Frequency Cross Attention mechanism, comprising two components: B^{Re} and B^{Im} . Here, B^{Re} captures the ability of the real part to preserve the information of the imaginary part, while B^{Im} quantifies how well the imaginary part can transform into the real part, as depicted in Figure 2. To enable the model to jointly attend to information from different representation subspaces, we use H heads of cross-attention mechanisms. For the h -th head, we apply linear mappings to transform the real part Re into Q_h^{Re} , K_h^{Re} , and V_h^{Re} , and the imaginary part Im into Q_h^{Im} , K_h^{Im} , and V_h^{Im} :

$$\begin{aligned} Q_h^{\text{Re}} &= \text{Re}^T W_h^{\text{Re},Q} + b_h^{\text{Re},Q}, Q_h^{\text{Im}} = \text{Im}^T W_h^{\text{Im},Q} + b_h^{\text{Im},Q}, \\ K_h^{\text{Re}} &= \text{Re}^T W_h^{\text{Re},K} + b_h^{\text{Re},K}, K_h^{\text{Im}} = \text{Im}^T W_h^{\text{Im},K} + b_h^{\text{Im},K}, \\ V_h^{\text{Re}} &= \text{Re}^T W_h^{\text{Re},V} + b_h^{\text{Re},V}, V_h^{\text{Im}} = \text{Im}^T W_h^{\text{Im},V} + b_h^{\text{Im},V}. \end{aligned} \quad (10)$$

Here, $W_h^{*,Q/K} \in \mathbb{R}^{D \times d_K}$, $W_h^{*,V} \in \mathbb{R}^{D \times d_V}$, $b_h^{*,Q/K} \in \mathbb{R}^{d_K}$, and $b_h^{*,V} \in \mathbb{R}^{d_V}$ are learnable parameters. Additionally, $Q_h^*, K_h^* \in \mathbb{R}^{P \times M \times d_K}$, $V_h^* \in \mathbb{R}^{P \times M \times d_V}$. When computing $\text{Attn}_h^{\text{Im}}$, the representation of the real part Re is augmented with the imaginary part Im . Conversely, while calculating $\text{Attn}_h^{\text{Re}}$, the representation of the real part Re needs to be modulated by learnable weights in conjunction with the imaginary part Im :

$$\begin{aligned} \text{Attn}_h^{\text{Re}}(Q_h^{\text{Re}}, K_h^{\text{Re}}, V_h^{\text{Im}}) &= \text{softmax}\left(\frac{Q_h^{\text{Re}}(K_h^{\text{Re}})^T}{\sqrt{d_K}}\right)V_h^{\text{Im}}, \\ \text{Attn}_h^{\text{Im}}(Q_h^{\text{Im}}, K_h^{\text{Im}}, V_h^{\text{Re}}) &= \text{softmax}\left(\frac{Q_h^{\text{Im}}(K_h^{\text{Im}})^T}{\sqrt{d_K}}\right)V_h^{\text{Re}}. \end{aligned} \quad (11)$$

After computing the attention weight matrices for all H attention heads, we concatenate all $\text{Attn}_h^{\text{Re}}$ and $\text{Attn}_h^{\text{Im}}$ and then apply linear transformations to map them to the augmented imaginary part $\tilde{\text{Im}} \in \mathbb{R}^{P \times M \times d_{\text{hidden}}}$ and real part $\tilde{\text{Re}} \in \mathbb{R}^{P \times M \times d_{\text{hidden}}}$.

$$\begin{aligned}\tilde{\text{Im}} &= \text{MultiHead}(Q^{\text{Re}}, K^{\text{Re}}, V^{\text{Im}}) = \text{Concat}(\text{Attn}_1^{\text{Re}}, \dots, \text{Attn}_H^{\text{Re}})W^{\text{Im}}, \\ \tilde{\text{Re}} &= \text{MultiHead}(Q^{\text{Im}}, K^{\text{Im}}, V^{\text{Re}}) = \text{Concat}(\text{Attn}_1^{\text{Im}}, \dots, \text{Attn}_H^{\text{Im}})W^{\text{Re}}.\end{aligned}\tag{12}$$

Here, the projections $W^{\text{Re}}, W^{\text{Im}} \in \mathbb{R}^{Hd_V \times d_{\text{hidden}}}$ are learnable parameter matrices.

3.3 Fi²VBlock

As shown in Figure 2, we organize the Fi²VBlock in a residual manner to form Fi²VTS, inspired by [He et al., 2016]. Specifically, for input time series $X \in \mathbb{R}^{D \times L}$, we first apply the normalization at the very beginning of Fi²VTS to address the nonstationary characteristics resulting from varying mean μ_X and standard deviation σ_X . At the end of the Fi²VTS, denormalization is applied to transform the model outputs back to the original statistics, as suggested by [Liu et al., 2022]. After normalization, we then utilize a linear embedding layer to project the inputs into deep features $X^0 \in \mathbb{R}^{E \times L}$. For the n -th Fi²VBlock of the Fi²VTS with the input $X^{n-1} \in \mathbb{R}^{E \times L}$, the process can be described as follows:

$$X^n = \text{Fi}^2\text{VBlock}^n(X^{n-1}) + X^{n-1}.\tag{13}$$

As depicted in Figure 2, in the n -th Fi²VBlock, the process consists of two successive phases in the frequency domain: capturing intra-variable variations and integrating inter-variable information.

3.3.1 Capturing Intra-variable Variations

In each Fi²VBlock, we sequentially apply the Frequency Transform Module (FTM) followed by the Frequency Cross Attention (FCA). The deep features $X^{n-1} \in \mathbb{R}^{E \times L}$ are first processed by the FTM to obtain the Top-M real and imaginary parts in the frequency domain. Subsequently, the FCA is used to connect the real part $\tilde{\text{Re}}$ and the imaginary part $\tilde{\text{Im}}$, capturing intra-variable variations effectively. The formalized procedure is as follows:

$$\begin{aligned}\text{Re}^n, \text{Im}^n &= \text{FTM}^n(X^{n-1}), \\ \tilde{\text{Re}}^n, \tilde{\text{Im}}^n &= \text{FCA}^n(\text{Re}^n, \text{Im}^n),\end{aligned}\tag{14}$$

where $\text{Re}^n, \text{Im}^n \in \mathbb{R}^{E \times P \times M}$ are the selected real and imaginary parts obtained by encoding X^{n-1} through the FTM. $\tilde{\text{Re}}^n, \tilde{\text{Im}}^n \in \mathbb{R}^{P \times M \times d_{\text{hidden}}}$ represent the augmented real and imaginary parts.

3.3.2 Integrating Inter-variable Information

After the FCA, we concatenate the real and imaginary parts and then process them through a linear mapping Linear^n with learnable parameters $W^n \in \mathbb{R}^{d_{\text{hidden}} \times E}$ and $b^n \in \mathbb{R}^E$. Subsequently, we pass the result through parameter-efficient Inception blocks [Szegedy et al., 2015] denoted as $\text{Inception}^n(\cdot)$, which incorporates multi-scale kernels and is widely recognized as a prominent architectural component in computer vision. The learned representations serve as the output of the n -th Fi²VBlock, combining inter-variable information that captures correlations between variables through their mutual influences.

$$\hat{X}^n = \text{Inception}^n(\text{Linear}^n(\text{Concat}(\tilde{\text{Re}}^n, \tilde{\text{Im}}^n))),\tag{15}$$

3.4 Efficient computation

For each Fi²VBlock, the time complexity is the sum of the time complexity of the STFT in the Frequency Transform Module and the attention mechanism in the Frequency Cross Attention. The time complexity of the STFT, with a window size of W , is typically expressed as $\mathcal{O}(W \log W)$. This is because applying the FFT to each window requires computational effort of $\mathcal{O}(W \log W)$. For time series with length L and D variables, the total time complexity for P windows is $\mathcal{O}(\sum_{p=1}^P LDW \log W)$. Since W, D, P are usually predefined constants and are typically much smaller than L , the time complexity is finally $\mathcal{O}(L)$.

On the other hand, the memory complexity of Fi^2VTS depends on the requirements for storing intermediate results in the STFT and attention weight matrices in the Frequency Cross Attention. For the STFT, the FFT results must be stored for each window, which incurs a memory cost of $\mathcal{O}(\sum_{p=1}^P DL)$. Consequently, the memory complexity of the Frequency Cross Attention is mainly due to the storage of attention weights and intermediate results. However, since the Frequency Transform Module standardizes the input size for Frequency Cross Attention, represented as $\text{Re}^n, \text{Im}^n \in \mathbb{R}^{E \times P \times M}$, where E, P, M are predefined hyperparameters, the complexity of Frequency Cross Attention in this work is $\mathcal{O}(EPM) = \mathcal{O}(1)$. Given that D and P are generally predefined constants and typically much smaller than L , the memory complexity of Fi^2VTS is thus $\mathcal{O}(L)$.

4 Experiments

In this section, we compare the well-acknowledged and advanced models in time series forecasting, including the CNN-based model: TimesNet [Wu et al., 2023]; MLP-based models: LightTS [Zhang et al., 2022], DLinear [Zeng et al., 2023], FreTS [Yi et al., 2023] and FITS [Xu et al., 2024]; Transformer-based models: Autoformer [Wu et al., 2021], FEDformer [Zhou et al., 2022], NSformer [Liu et al., 2022], ETSformer [Woo et al., 2022], PatchTST [Nie et al., 2023], Crossformer [Zhang and Yan, 2023] and iTransformer [Liu et al., 2024]. Overall, 12 baselines are included for a comprehensive comparison.

4.1 Datasets

We evaluate the performance of Fi^2VTS on two widely acknowledged time series simulators with parameter localization based on real-world data, covering mainstream applications in TSF: medicine (the Type 1 Diabetes Mellitus Simulator (T1DMs) [Man et al., 2014]) and agriculture (the Lintul3 [Shibu et al., 2010]).

- The Type 1 Diabetes Mellitus Simulator (T1DMs) [Man et al., 2014] elucidates the temporal evolution of patient states in response to different distributions of exogenous insulin intervention doses. The U.S. Food and Drug Administration has accepted this simulator as a viable alternative to preclinical testing for evaluating novel treatment modalities for Type 1 Diabetes Mellitus. In this study, simulations are performed using default settings tailored for adult patients to generate temporal data sequences.
- Lintul3 [Shibu et al., 2010] is a classic crop growth model. In this experiment, we simulated the growth process of spring wheat in Northeast China in 2002. The dataset includes 20 time-series variables, including two dimensions of action variables and 18 dimensions of crop trait variables.

We follow standard protocol and split all datasets into training, validation, and test sets in chronological order by the ratio 7:1:2 for all datasets. We adhere to the experimental settings established in TimesNet [Wu et al., 2023] and Autoformer [Wu et al., 2021] for a fair comparison.

4.2 Evaluation Metrics

We use the mean square error (MSE) and mean absolute error (MAE) to evaluate the accuracy of TSF, which is calculated as follows:

$$\begin{aligned} \text{MSE}(\hat{X}, X) &= \frac{1}{D \times T} \sum_{j=1}^D \sum_{t=L+1}^{L+T} (\hat{x}_j^t - x_j^t)^2 \\ \text{MAE}(\hat{X}, X) &= \frac{1}{D \times T} \sum_{j=1}^D \sum_{t=L+1}^{L+T} |\hat{x}_j^t - x_j^t| \end{aligned} \tag{16}$$

Here, $\hat{X} \in \mathbb{R}^{D \times T}$ represents the estimated time series, while X denotes the corresponding ground-truth. The lower MSEs and MAEs indicate a better model for time series forecasting.

4.3 Implementation details

Similar to TimesNet [Wu et al., 2023], our proposed model, Fi^2VTS , employs L2 loss for training and is optimized using the Adam optimizer with an initial learning rate of 10^{-3} . The batch size is configured to 32. All experiments are repeated five times, implemented in PyTorch, and conducted on a single NVIDIA RTX TITAN 24GB GPU.

Table 1: The MSEs and MAEs of the time series forecasting. The cumulative number of first-place predictions for each model is summarized in the last row, serving as a comprehensive metric for evaluating overall model performance. The best results are highlighted in bold, while the second-best results are underlined.

Models	Fi ² VTS		iTransformer		FITS		Crossformer		FreTS		TimesNet		PatchTST		DLinear		ETSformer		FEDformer		NSformer		LightTS		Autoformer		
	MSE	MAE	MSE	MAE	MSE	MAE	MSE	MAE	MSE	MAE	MSE	MAE	MSE	MAE	MSE	MAE	MSE	MAE	MSE	MAE	MSE	MAE	MSE	MAE	MSE	MAE	
T1DMs	96	0.06	0.03	0.409	0.22	0.853	0.514	0.23	0.52	0.291	0.171	0.13	<u>0.06</u>	0.475	0.265	0.39	0.32	0.17	0.18	0.07	0.08	0.19	0.11	0.07	0.07	0.28	0.26
	192	<u>0.08</u>	0.11	0.429	0.273	1.044	0.618	0.19	0.59	0.257	0.199	0.12	0.07	0.649	0.372	0.43	0.36	0.34	0.33	0.06	<u>0.10</u>	0.20	0.15	0.12	0.07	0.56	0.45
	336	<u>0.07</u>	0.11	0.419	0.286	1.099	0.652	0.28	0.66	0.273	0.237	0.10	0.07	0.591	0.388	0.45	0.39	0.49	0.44	0.06	0.12	0.16	0.14	0.15	<u>0.09</u>	0.33	0.31
	720	0.07	<u>0.11</u>	0.382	0.265	0.962	0.518	0.22	0.71	0.233	0.206	0.11	0.09	0.583	0.371	0.38	0.34	0.56	0.47	0.12	0.20	0.20	0.15	0.60	<u>0.50</u>	0.60	0.46
	Avg	0.07	<u>0.09</u>	0.409	0.261	0.989	0.575	0.20	0.62	0.263	0.203	0.12	0.07	0.582	0.349	0.41	0.35	0.39	0.35	<u>0.08</u>	0.12	0.19	0.14	0.24	0.18	0.44	0.37
Lintul3	7	2.81	0.42	159.55	4.44	238.09	10.21	58.96	5.14	133.82	5.71	5.72	0.77	176.70	7.52	172.22	6.42	59.94	3.40	23.32	1.99	6.73	0.82	<u>3.69</u>	0.77	15.32	1.62
	14	2.87	0.60	259.31	12.10	411.18	15.31	60.42	5.42	250.35	11.03	12.85	0.96	325.21	11.41	366.81	9.22	43.23	2.96	10.77	1.51	19.03	1.19	13.69	1.35	75.06	3.24
	21	2.49	0.81	447.08	12.87	606.52	20.41	59.02	5.81	364.99	15.55	28.86	1.28	462.60	15.30	600.12	11.75	135.42	4.89	11.31	1.50	21.17	0.99	8.01	1.21	90.10	3.48
	30	4.56	0.99	672.39	18.37	866.90	26.64	59.87	6.03	482.04	19.97	64.22	1.85	647.39	19.44	861.78	14.02	82.08	3.58	12.48	1.52	34.37	1.18	<u>10.40</u>	1.34	305.86	5.92
	Avg	3.18	0.71	384.58	11.94	530.67	18.14	59.57	5.60	307.80	13.06	27.91	1.21	402.97	13.42	500.23	10.35	80.16	3.70	14.47	1.63	20.33	<u>1.05</u>	<u>8.94</u>	1.16	121.59	3.57
1 st Count	14		0		0		0		0		<u>4</u>		0		0		0		2		0		1		0		

We specify the embedding dimension E to 32, allowing us to map the input $X \in \mathbb{R}^{D \times L}$ to the embedding $X^0 \in \mathbb{R}^{32 \times L}$. To mitigate degradation issues, we utilize $N = 4$ Fi²VBlocks, incorporating residual connections. Each Fi²VBlock employs $P = 3$ windows with sizes $W = \{100, 50, 20\}$, all configured as Hann windows. We select $M = 10$ from the STFT results for each window to enhance computational efficiency. The dimensions d_K , d_V , and d_{hidden} in the Frequency Cross Attention are uniformly set to 64. Within the Inception blocks, we use six kernels of varying sizes to integrate inter-variable information from distinct STFT windows. Our findings suggest that the dimensions of the hidden layers and the number of kernels do not significantly influence the performance of Fi²VTS. Consequently, we undertake ablation studies on the number of Fi²VBlocks N , the embedding dimension E , the window W , and the selector M .

4.4 Main Results

The results of TSF are summarized in Table 1. We count the cumulative number of first-place predictions achieved by each model across various datasets, providing a comprehensive metric for evaluating overall model performance. The best results are highlighted in bold, while the second-best results are underlined.

Experimental results reveal that Fi²VTS performs best across all benchmark datasets. Specifically, Fi²VTS delivers state-of-the-art performance in 75% of all cases. On the T1DMs dataset, all methods perform relatively well. Notably, TimesNet, LightTS, and FEDformer achieve lowest MSEs and MAEs. One possible reason is that the T1DMs dataset, which reflects blood glucose levels in the human body, typically shows an upward trend before and after meals, followed by a decline to a stable level, forming a highly regular pattern. However, Fi²VTS remains the best model overall, obtaining the lowest average MSE and the second-lowest average MAE. The experimental results on the Lintul3 dataset significantly demonstrate the superiority of Fi²VTS. It not only achieves the highest accuracy for every forecasting length but also maintains this accuracy consistently across different lengths, thereby validating the stability of Fi²VTS. We attribute this predictive accuracy and performance stability to the design of the Frequency Cross Attention, which effectively captures intra-variable variations.

4.5 Model Efficiency Analysis

In our model efficiency analysis, we believe that analyzing the parameter scale and GPU memory size is only necessary when a model demonstrates high accuracy. Additionally, since prediction lengths may vary across different datasets, leading to changes in parameter scale and GPU memory size, we choose to compare the parameter scale and GPU memory size of Fi²VTS, iTransformer, FITS, FreTS, TimesNet and PatchTST on the ETTh1 dataset. These six methods have achieved the lower MSEs and MAEs on three datasets compared to others.

Among these models, our proposed Fi²VTS and TimesNet exhibit nearly identical parameter sizes and GPU memory usage, with parameter sizes of 4.6MB and 4.5MB and GPU memory sizes of 1703MiB for both. On the other hand, the MLP-based model, FreTS, has relatively smaller parameter sizes and GPU memory usage, averaging around 0.04MB and 1699MiB, while FITS only requires 10k parameters. However, MLP-based models may struggle to simulate time series data effectively due to their small parameter size. Conversely, PatchTST and iTransformer have parameter sizes and GPU memory usage similar to MLP-based models, but they fail to capture extreme values in time series data. We attribute the larger parameter size of Fi²VTS primarily to the Inception blocks used in each Fi²VBlock, which subsequently increases the parameters. Despite this, Fi²VTS achieves the best performance within an acceptable single-GPU model size despite the increased parameter count.

5 Conclusion, Limitations and Future Works

In this paper, we propose Fi²VTS that leverages Fi²VBlocks connected in a residual way, resulting in state-of-the-art performance. Each Fi²VBlock employs the STFT for the multi-period signal analysis, facilitating the acquisition of intra-variable variations from a frequency perspective. Inspired by KKR, we propose Frequency Cross Attention between the real and imaginary parts to obtain enhanced frequency representations and capture intra-variable variations. Inception blocks are further used to mix information to capture correlations between variables. Extensive experiments demonstrate that Fi²VTS achieves superior forecasting performance with minimal resource consumption on three benchmark datasets, outperforming 12 state-of-the-art algorithms. Furthermore, Fi²VTS reduces the time and memory complexity of each Fi²VBlock computation from $\mathcal{O}(L^2)$ to $\mathcal{O}(L)$.

While Fi²VTS demonstrates exceptional performance, there are still some limitations. For example, Fi²VTS may incorrectly categorize mutations in time-series data as noise and overlook the accurate modeling of simple periodic curves. Therefore, to further improve and overcome the limitations, we intend to utilize both time- and frequency-domain information to improve model performance. In addition, we aim to explore large-scale pre-training methods tailored explicitly to time series applications, using Fi²VTS as the underlying architecture. This approach can potentially bring significant benefits to a wide range of downstream tasks.

6 Acknowledgments

This study was supported in part by a grant from the National Key Research and Development Program of China [2021ZD0110900] and the National Natural Science Foundation of China [62006063].

References

- Haixu Wu, Jiehui Xu, Jianmin Wang, and Mingsheng Long. Autoformer: Decomposition transformers with auto-correlation for long-term series forecasting. In *Advances in Neural Information Processing Systems*, 2021.
- Yong Liu, Haixu Wu, Jianmin Wang, and Mingsheng Long. Non-stationary transformers: Exploring the stationarity in time series forecasting. In *Advances in Neural Information Processing Systems*, 2022.
- Tian Zhou, Ziqing Ma, Qingsong Wen, Xue Wang, Liang Sun, and Rong Jin. FEDformer: Frequency enhanced decomposed transformer for long-term series forecasting. In *Proc. 39th International Conference on Machine Learning (ICML 2022)*, 2022.
- Gerald Woo, Chenghao Liu, Doyen Sahoo, Akshat Kumar, and Steven Hoi. Etsformer: Exponential smoothing transformers for time-series forecasting. *arXiv preprint arXiv:2202.01381*, 2022.
- Yuqi Nie, Nam H. Nguyen, Phanwadee Sinthong, and Jayant Kalagnanam. A time series is worth 64 words: Long-term forecasting with transformers. In *International Conference on Learning Representations*, 2023.
- Yong Liu, Tengge Hu, Haoran Zhang, Haixu Wu, Shiyu Wang, Lintao Ma, and Mingsheng Long. itransformer: Inverted transformers are effective for time series forecasting. In *The Twelfth International Conference on Learning Representations*, 2024.
- Zhijian Xu, Ailing Zeng, and Qiang Xu. FITS: Modeling time series with \$10k\$ parameters. In *The Twelfth International Conference on Learning Representations*, 2024.
- Li Li, Jie Sun, Liemin Ruan, and Qifa Song. Time-series analysis of continuous glucose monitoring data to predict treatment efficacy in patients with t2dm. *The Journal of Clinical Endocrinology & Metabolism*, 106(8):2187–2197, 2021.
- Heydar Khadem, Hoda Nemat, Jackie Elliott, and Mohammed Benaissa. Blood glucose level time series forecasting: Nested deep ensemble learning lag fusion. *Bioengineering*, 10(4):487, 2023.
- Umesh Saini, Rajesh Kumar, Vipin Jain, and MU Krishnajith. Univariate time series forecasting of agriculture load by using lstm and gru rnns. In *2020 IEEE Students Conference on Engineering & Systems (SCES)*, pages 1–6. IEEE, 2020.
- Yunhao Zhang and Junchi Yan. Crossformer: Transformer utilizing cross-dimension dependency for multivariate time series forecasting. In *The Eleventh International Conference on Learning Representations*, 2023.
- Kun Yi, Qi Zhang, Wei Fan, Shoujin Wang, Pengyang Wang, Hui He, Ning An, Defu Lian, Longbing Cao, and Zhendong Niu. Frequency-domain MLPs are more effective learners in time series forecasting. In *Thirty-seventh Conference on Neural Information Processing Systems*, 2023.

- George EP Box and Gwilym M Jenkins. Some recent advances in forecasting and control. *Journal of the Royal Statistical Society. Series C (Applied Statistics)*, 17(2):91–109, 1968.
- George EP Box, Gwilym M Jenkins, Gregory C Reinsel, and Greta M Ljung. *Time series analysis: forecasting and control*. John Wiley & Sons, 2015.
- Larry R Medsker and LC Jain. Recurrent neural networks. *Design and Applications*, 5(64-67):2, 2001.
- Yoshua Bengio, Patrice Simard, and Paolo Frasconi. Learning long-term dependencies with gradient descent is difficult. *IEEE transactions on neural networks*, 5(2):157–166, 1994.
- Sepp Hochreiter and Jürgen Schmidhuber. Long short-term memory. *Neural computation*, 9(8):1735–1780, 1997.
- Junyoung Chung, Caglar Gulcehre, Kyunghyun Cho, and Yoshua Bengio. Empirical evaluation of gated recurrent neural networks on sequence modeling. In *NIPS 2014 Workshop on Deep Learning, December 2014*, 2014.
- Ashish Vaswani, Noam Shazeer, Niki Parmar, Jakob Uszkoreit, Llion Jones, Aidan N Gomez, Łukasz Kaiser, and Illia Polosukhin. Attention is all you need. *Advances in neural information processing systems*, 30, 2017.
- Jacob Devlin Ming-Wei Chang Kenton and Lee Kristina Toutanova. Bert: Pre-training of deep bidirectional transformers for language understanding. In *Proceedings of naacL-HLT*, volume 1, page 2, 2019.
- Alexey Dosovitskiy, Lucas Beyer, Alexander Kolesnikov, Dirk Weissenborn, Xiaohua Zhai, Thomas Unterthiner, Mostafa Dehghani, Matthias Minderer, Georg Heigold, Sylvain Gelly, et al. An image is worth 16x16 words: Transformers for image recognition at scale. In *International Conference on Learning Representations*, 2020.
- Haixu Wu, Tengge Hu, Yong Liu, Hang Zhou, Jianmin Wang, and Mingsheng Long. Timesnet: Temporal 2d-variation modeling for general time series analysis. In *International Conference on Learning Representations*, 2023.
- Christian Szegedy, Wei Liu, Yangqing Jia, Pierre Sermanet, Scott Reed, Dragomir Anguelov, Dumitru Erhan, Vincent Vanhoucke, and Andrew Rabinovich. Going deeper with convolutions. In *Proceedings of the IEEE conference on computer vision and pattern recognition*, pages 1–9, 2015.
- Tianping Zhang, Yizhuo Zhang, Wei Cao, Jiang Bian, Xiaohan Yi, Shun Zheng, and Jian Li. Less is more: Fast multivariate time series forecasting with light sampling-oriented mlp structures. *arXiv preprint arXiv:2207.01186*, 2022.
- Ailing Zeng, Muxi Chen, Lei Zhang, and Qiang Xu. Are transformers effective for time series forecasting? 2023.
- Henri J Nussbaumer and Henri J Nussbaumer. *The fast Fourier transform*. Springer, 1982.
- William T Cochran, James W Cooley, David L Favin, Howard D Helms, Reginald A Kaenel, William W Lang, George C Maling, David E Nelson, Charles M Rader, and Peter D Welch. What is the fast fourier transform? *Proceedings of the IEEE*, 55(10):1664–1674, 1967.
- William L Briggs and Van Emden Henson. *The DFT: an owner’s manual for the discrete Fourier transform*. SIAM, 1995.
- Zoran Cvetkovic. On discrete short-time fourier analysis. *IEEE transactions on signal processing*, 48(9):2628–2640, 2000.
- Lutfiye Durak and Orhan Arikan. Short-time fourier transform: two fundamental properties and an optimal implementation. *IEEE Transactions on Signal Processing*, 51(5):1231–1242, 2003.
- Kamran Karimi and Howard J Hamilton. Distinguishing causal and acausal temporal relations. In *Pacific-Asia Conference on Knowledge Discovery and Data Mining*, pages 234–240. Springer, 2003.
- Frederick W King. *Hilbert Transforms: Volume 2*, volume 2. Cambridge University Press, 2009.
- Vaclav Cizek. Discrete hilbert transform. *IEEE Transactions on Audio and Electroacoustics*, 18(4):340–343, 1970.
- D Benitez, PA Gaydecki, A Zaidi, and AP Fitzpatrick. The use of the hilbert transform in ecg signal analysis. *Computers in biology and medicine*, 31(5):399–406, 2001.
- Eric W Weisstein. Convolution theorem. *From MathWorld-A Wolfram Web Resource*, 2006a. URL <http://mathworld.wolfram.com/ConvolutionTheorem.html>, 2014.
- Kai Xu, Minghai Qin, Fei Sun, Yuhao Wang, Yen-Kuang Chen, and Fengbo Ren. Learning in the frequency domain. In *Proceedings of the IEEE/CVF conference on computer vision and pattern recognition*, pages 1740–1749, 2020.
- Kaiming He, Xiangyu Zhang, Shaoqing Ren, and Jian Sun. Deep residual learning for image recognition. In *Proceedings of the IEEE conference on computer vision and pattern recognition*, pages 770–778, 2016.
- Chiara Dalla Man, Francesco Micheletto, Dayu Lv, Marc Breton, Boris Kovatchev, and Claudio Cobelli. The uva/padova type 1 diabetes simulator: new features. *Journal of diabetes science and technology*, 8(1):26–34, 2014.
- Muhammed E Shibu, Peter A Leffelaar, Herman Van Keulen, and Pramod K Aggarwal. Lintul3, a simulation model for nitrogen-limited situations: Application to rice. *European Journal of Agronomy*, 32(4):255–271, 2010.